Proceedings of ASME Turbo Expo 2011
GT2011
June 6-10, 2011, Vancouver, British Columbia, Canada

GT2011-45645

SHOCK PROPAGATION AND MPT NOISE FROM A TRANSONIC ROTOR IN NON-UNIFORM FLOW

J. J. Defoe and Z. S. Spakovszky
MIT Gas Turbine Laboratory
Cambridge, MA 02139, USA

ABSTRACT

One of the major challenges in hig4h-speed fan stages used in compact, embedded propulsion systems is inlet distortion noise. A body-force-based approach for the prediction of multiple-pure-tone (MPT) noise was previously introduced and validated. In this paper, it is employed with the objective of quantifying the effects of non-uniform flow on the generation and propagation of MPT noise.

First-of-their-kind back-to-back coupled aero-acoustic computations were carried out using the new approach for conventional and serpentine inlets. Both inlets delivered flow to the same NASA/GE R4 fan rotor at equal corrected mass flow rates. Although the source strength at the fan is increased by 45 dB in sound power level due to the non-uniform inflow, far-field noise for the serpentine inlet duct is increased on average by only 3.1 dBA overall sound pressure level in the forward arc. This is due to the redistribution of acoustic energy to frequencies below 11 times the shaft frequency and the apparent cut-off of tones at higher frequencies including blade-passing tones. The circumferential extent of the inlet swirl distortion at the fan was found to be 2 blade pitches, or 1/11th of the circumference, suggesting a relationship between the circumferential extent of the inlet distortion and the apparent cut-off frequency perceived in the far field.

A first-principles-based model of the generation of shock waves from a transonic rotor in non-uniform flow showed that the effects of non-uniform flow on acoustic wave propagation, which cannot be captured by the simplified model, are more dominant than those of inlet flow distortion on source noise. It demonstrated that non-linear, coupled aerodynamic and aero-acoustic computations, such as those presented in this paper, are necessary to assess the propagation through non-uniform mean flow. A parametric study of serpentine inlet designs is underway to quantify these propagation effects.

NOMENCLATURE

A	Area
B	Number of fan blades
c	Speed of sound
C_n	Spatial Fourier coefficient of sawtooth wave
D	Downstream diameter of serpentine duct
f	Body force per unit volume
g	Solution to Helmholtz equation
I	Sound intensity
j	Imaginary number, $\sqrt{-1}$
k	Wavenumber
L	Axial length of serpentine duct
m	Circumferential mode of inlet distortion
M	Mach number
M_1	Relative Mach number upstream of rotor
M_2	Relative Mach number in blade passage
M_∞	Free-stream Mach number
M_u	Rotor wheel Mach number
n	Circumferential mode of sawtooth wave
N	Unit-amplitude sawtooth wave
p	Static pressure
p_t	Stagnation pressure
P_m	Spatial Fourier coefficient of inlet distortion
r	Radial coordinate
R	Duct radius
s	Staggered gap
S	Dimensionless body force perturbation
t	Time
T	Static temperature
$\bar{u}$	Average velocity
V	Velocity
x	Axial coordinate
α	Blade metal angle
β_1	Relative flow angle upstream of fan
γ	Ratio of specific heats
δ	Vertical offset of serpentine duct

δf	Body force perturbation
ε	MPT-generating body force perturbation
θ	Circumferential coordinate
Θ_{em}	Emission angle
Θ_{geom}	Geometric angle
Λ_{mn}	Compound Fourier coefficient
π_{12}	Static pressure ratio across detached shock
ρ	Density
χ_1	Leading-edge blade stagger angle
Ω	Fan rotational speed

INTRODUCTION AND BACKGROUND

The use of boundary layer-ingesting serpentine engine inlets has been identified [1-2] as one means to reduce fuel consumption on next-generation aircraft, but there is limited quantitative understanding of how the distorted inflow influences the upstream-propagating fan noise. For transonic fans, the upstream-propagating noise is comprised of fan broadband and tonal noise, which consists of blade-passing frequency (BPF) and interaction tones plus higher harmonics. It also includes multiple-pure-tone (MPT) noise, so called "buzz-saw noise," found at multiples of shaft frequency. MPT noise occurs at supersonic blade-tip flow conditions and is due to irregularities in the upstream rotor shock system caused by small variations in blade stagger angle. These can stem from imperfections in the blade manufacturing and installation processes, and can be as much as $\pm 0.2°$ [3]. The focus of this paper is particularly on forward radiating MPT and BPF tone noise, referred to here in short as rotor-alone tone noise.

A key challenge associated with predicting the rotor-alone tone generation and propagation in distorted inflow is the coupling of the aerodynamics and acoustics and the non-linear nature of the related processes. To properly treat the problem, the flow field, sound generation and noise propagation must be computed simultaneously to capture their interactions. To date, there has been no quantification of the degree to which inlet distortion and non-uniform flow can alter the generation and propagation of fan noise. Although studies exist on some aspects of this problem in the open literature, a fully coupled analysis and back-to-back comparison with clean inlet flow has not yet been reported.

Mathews and Nagel [4] developed an analytical model for shock propagation in circular ducts with variable cross-sectional area by modeling the shocks as sawtooth waves. This approach enables an approximate prediction of the shock decay rate in any axisymmetric inlet but does not account for three-dimensional flow effects which become important in serpentine inlet ducts.

Prasad and Feng [5] numerically predicted the propagation of upstream-traveling waves in a conventional axisymmetric inlet. 3D flow effects were assessed by examining two inlets which varied only in their throat areas. The increased local flow accelerations near the nacelle on the reduced-throat area inlet resulted in additional noise attenuation not predicted by the simplified model of Mathews and Nagel.

Gliebe et al. [3] used a decoupled approach to model MPT noise generation and propagation. Though this approach is useful for uniform inflow, the assumed lack of coupling between the propagating waves and the mean flow does not hold for non-uniform inflow.

Coupland et al. [6] performed a high-fidelity simulation on an axisymmetric inlet with varying blade stagger angles to generate MPT noise, and propagated the noise through the inlet and to the exterior surface of the aircraft cabin in order to assess the cabin interior MPT noise. While the approach made no simplifying assumptions the computational cost prohibits parametric studies—the grid used consisted of over 55 million cells.

Brambley and Peake [7-8] investigated the propagation of linear acoustic waves through circular and annular ducts with strong curvature and a slowly-varying cross-sectional area. Although the approach assumed inviscid, irrotational flow and did not include the noise generation process, concentration of acoustic energy near the duct walls was observed, conjectured to be due to competing effects between the curved geometry and the refraction caused by the mean flow.

In summary, computing the generation and propagation of MPT noise in serpentine inlet ducts requires a non-linear, fully coupled aero-acoustic approach. In the presence of boundary layer ingestion (BLI) and inlet swirl distortion, the method must also be capable of dealing with non-uniform rotational flows and their interaction with the fan rotor. A methodology meeting all of the above requirements has recently been developed and demonstrated on a conventional inlet-fan system [9]. This method is used here for a serpentine inlet duct. To complement the simulations a simplified model for the rotor-alone tone noise generation is established, with the goal of gaining insight into whether it is the inlet distortion effects on acoustic source generation or the wave propagation through non-uniform flow which governs the acoustic behavior and perceived noise in the far-field.

SCOPE OF THE PAPER

The main objectives of this paper are (1) to quantify the effect of inlet swirl distortion on the generation and propagation of multiple-pure-tone noise in serpentine inlet systems relative to uniform inflow conditions, and (2) to characterize and to dissect the underlying mechanisms responsible for the changes in source noise and the noise radiating from the inlet system. It will be shown that the source noise sound power is increased by as much as 45 dB due to the swirling inflow at the fan face while on average the overall A-weighted sound pressure level (OASPL) in the far-field is only increased by 3 dBA. The detailed interpretation and interrogation of these results is the focus of this paper. It is conjectured that the local shock strength is increased in regions of counter-swirl while the sound power decay is enhanced in regions of subsonic relative Mach number induced by the co-rotating streamwise vorticity and the altered propagation characteristics of the non-uniform flow in the serpentine inlet duct. The far-field spectra show that the BPF tones are cut-off with inlet distortion and that acoustic energy is redistributed and increased at frequencies below 11 times shaft order frequency. In light of these findings, the following research questions are addressed in detail: (1) what is the impact of inlet swirl distortion on multiple-pure tone noise generation, (2) how does the non-uniform flow in the serpentine inlet duct affect far-field noise, and (3) are the effects of non-uniform flow on source noise dominant relative to its effects on acoustic propagation?

The technical approach employs a new methodology for the coupled aeroacoustic assessment of MPT noise using an innovative implementation of a body-force-based rotor model. A short overview is given below and more details of the methodology can be found in [9-10]. The high-fidelity numerical simulations, previously validated with experimental data acquired in the NASA SDT fan diagnostic tests [11-14], are supported by first-principles-based models for source noise generation and near-field acoustic propagation. The ultimate goal is to establish design guidelines in order to take advantage of the underlying mechanisms to alter the duct geometry and mean flow features to reduce far-field noise. A parametric study for a range of serpentine inlets is currently being carried out to determine the sensitivities and necessary flow conditions for reduced noise. The present paper quantifies for the first time the impact of inlet swirl distortion on MPT noise relative to that of the same fan rotor in a conventional inlet.

MODELING APPROACH

The framework and conceptual outline of the methodology is summarized in Fig. 1, applicable for both conventional and serpentine inlet duct configurations.

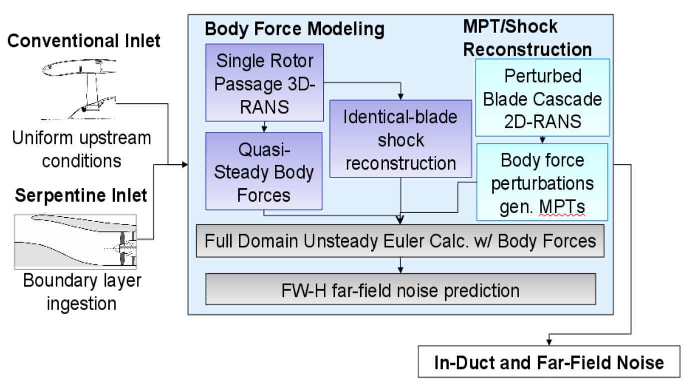

Fig. 1: MPT Noise prediction framework.

The key idea is to represent the fan rotor with a rotating body force field that generates MPT and BPF tone source noise while its time-mean component provides the quasi-steady pressure rise and flow turning. A single-passage, steady 3D RANS calculation of the fan rotor is first carried out to obtain the body-force-based description of the blade row performance. This body force field can respond locally to the flow conditions such that the effects of inlet distortion are captured. The body force field is then perturbed by a rotor-locked disturbance to create BPF tone noise. As shown in Fig. 2 this perturbation, its shape derived from the 3D RANS calculation, is periodic in blade pitch and generates the blade leading edge shock and expansion fan. In addition, a rotating disturbance field with once-per-revolution periodicity is introduced to generate variations in this shock system and thus MPT noise. The amplitude of the variations was obtained from a perturbed 2-D cascade RANS calculation. The complete body force formulation can then be summarized as follows, illustrated here for the x-body force component

$$f_x(r,x,\theta,t) = \bar{f}_x(M_{rel}(r,x,\theta), \alpha(r,x)) + \delta f_x(r,x,\theta-\Omega t) \quad (1)$$

where

$$\delta f_x(r,x,\theta-\Omega t) = \bar{f}_x(M_{rel},\alpha)\cdot(1+\varepsilon)\cdot S(r,x,\theta-\Omega t) \quad (2)$$

Here ε is the perturbation due to stagger angle changes from one blade passage to another and S is the perturbation function shown in Fig. 2.

This body force formulation is then implemented in a full domain unsteady Euler calculation and the far field noise is determined via the Ffowcs-Williams and Hawkings (FW-H) integral method using a permeable surface. A more detailed description and validation of this approach using 3D CFD calculations and experimental data can be found in [9].

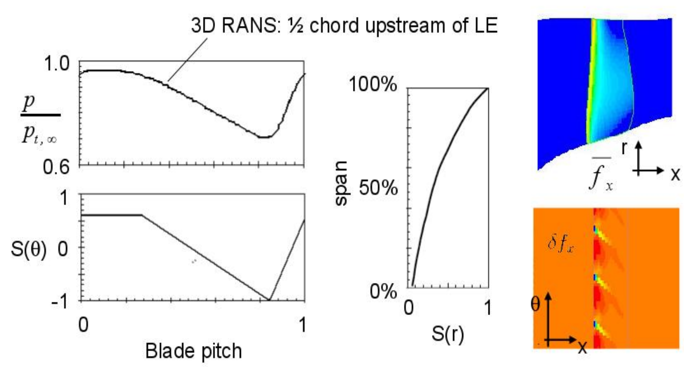

Fig. 2: Body force perturbation to generate rotor blade shocks.

Nacelle and Fan Geometry Definitions

In this paper, the body force approach is implemented for two engine installation configurations, a conventional axisymmetric inlet for high-bypass ratio fan engines and a serpentine inlet for an integrated propulsion system configuration with boundary layer ingestion. The same fan blade stagger angle variation is employed for both cases. Both inlets are coupled to the same fan rotor. For all computations, the NASA/GE R4 rotor with 22 rotor blades was modeled at the cutback operating condition (87.5% corrected design speed). Blade-to-blade stagger angle variations of $\pm 0.2°$, as suggested by Gliebe et al. [3], were introduced randomly. The fan exit guide vanes were not included in this analysis although the methodology could be extended to capture blade-row interaction noise. However, this was not part of this investigation. A detailed description of the conventional inlet and the NASA / GE R4 rotor geometry can be found in [12]. The serpentine inlet was based on the propulsion system integration configuration for the SAX-40 hybrid-wing body aircraft. The inlet was designed for boundary layer ingestion and has an offset of $\delta / D = 0.5$, an area ratio of $A_{AIP} / A_{throat} = 1.03$, and a length-to-diameter ratio of $L / D = 2.0$. The aerodynamic performance and geometric details can be found in [15]. In both the conventional and serpentine inlet cases, the fan exhaust was ducted out of the computational domain to prevent fan exhaust noise from contributing to the far-field noise levels. In the experiments, a barrier wall was used to prevent fan exhaust noise from contaminating the far-field measurements [13].

Computational Setup

The computational domains include the rotor region, the upstream duct and inlet, and the external flow field as shown in Fig. 3. While the conventional inlet was exposed to free stream conditions, the aircraft centerbody suction surface and boundary layer were included in the serpentine inlet calculation. The suction surface boundary layer and related stagnation pressure deficit were defined 10 diameters upstream of the inlet using previous viscous 3-D airframe computations [16].

All numerical simulations were carried out using the commercial CFD software FLUENT. The inherent dissipation present in the inviscid, 2nd-order, density-based solver was characterized to account for the non-physical wave decay in the far-field noise levels using a method based on the work of Huttl et al. [17]. This dissipation is a function of the wave resolution, typically specified in points per wavelength (PPW). A detailed grid sensitivity study was also carried out to meet the requirements for acoustic wave propagation, resulting in the use of a grid with 25 PPW at BPF. The FW-H surface was placed approximately 1.5 fan diameters from the inlet throat in both computations. Both computational domains comprised approximately 16 million cells and employed a structured grid topology. Highly-uniform cells were used in the rotor region, inlet duct and in the near-field region up to the FW-H surface to provide a favorable numerical environment for acoustic wave propagation. Acoustic buffer zones were placed outside the FW-H surface and in the duct far downstream of the rotor to prevent spurious wave reflections. The buffer zone formulation used grid stretching and explicit damping following the work by Freund [18]. The stagnation pressure (including the airframe boundary layer stagnation pressure deficit) and the free-stream flow direction were prescribed at the upstream boundary of the domain. At the downstream boundary in the external flow domain the static pressure was set to determine the free-stream Mach number, which was set to 0.1[1].

For the internal flow domain, the static pressure at the boundary downstream of the rotor was used to set the corrected flow through the inlet. Since the R4 rotor has 22 blades, the time step size was set to 1/1320 of the rotor revolution period based on time-step studies which determined that 60 time-steps per period for the highest frequency of interest (BPF) were required for acoustic propagation.

In both computations, the same far-field measurement locations relative to the fan were used. Acoustic receivers were placed 4 fan diameters from the fan axis over emission angles $\Theta_{em} = \Theta_{geom} - \sin^{-1}\left(M_{\infty}\sin\left(\Theta_{geom}\right)\right)$ ranging from $25°$ to $90°$, measured from the fan axis from aft looking forward.

The unsteady computations were initialized from steady calculations and carried out until two rotor revolutions of periodic acoustic data were recorded at all receiver locations. This ensured sufficient resolution in the frequency domain to identify the MPT and BPF tones in the far-field spectra.

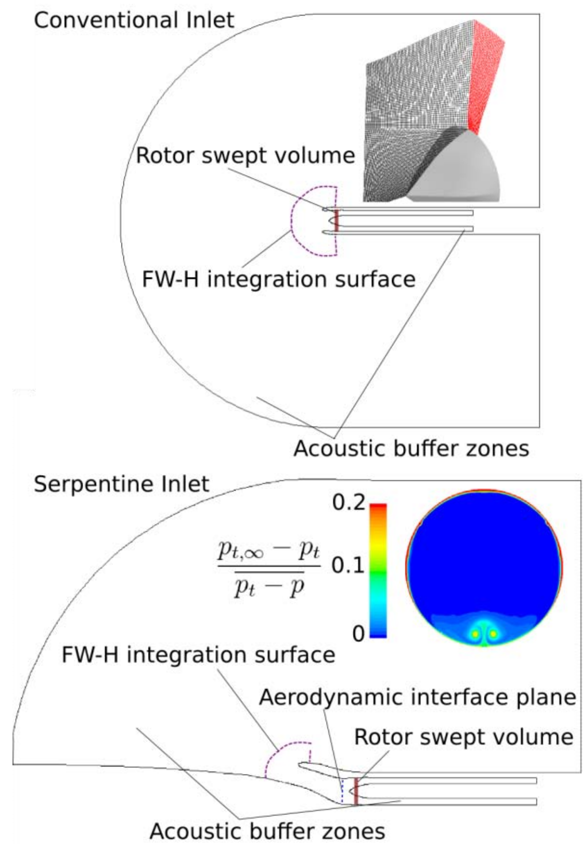

Fig. 3: Computational domains.

[1] Though the cut-back Mach number for the SAX-40 is 0.22, the free-stream Mach number of 0.1 is consistent with the experimental R4 wind tunnel data and is thus used throughout this work.

AERODYNAMIC AND AEROACOUSTIC RESULTS

The key results are summarized in Table 1. The sound power level was computed up to the blade passing frequency based on a modal decomposition of the unsteady pressure field, using the method by Sutliff [19]. The interaction of the inlet distortion and non-uniform flow through the serpentine inlet duct with the fan rotor increases the source noise by 45 dB in sound power (as opposed to sound pressure) relative to the conventional inlet case at the same fan operating conditions. However, there is enhanced sound power attenuation of 27 dB through the non-uniform flow from the fan to the aerodynamic interface plane (AIP) for the serpentine inlet case. The AIP corresponds to the inlet throat for the conventional inlet and for the serpentine inlet it is the farthest upstream location where the cross-section is circular. Both are at the same axial distance from the fan face. There is also a redistribution of acoustic energy to frequencies below 11 times shaft frequency. In particular the BPF tone and MPTs above 11 times shaft frequency are cut-off leading to an increase in far-field overall sound pressure level of only 7dB or 3dBA. To address the earlier stated objectives in light of these results, the in-duct aerodynamics, the rotor-alone noise and the noise propagation to far-field observers are dissected. Furthermore, the aero-acoustic features of the conventional inlet with axisymmetric flow conditions are carefully compared with the serpentine inlet to highlight important differences.

Table 1: In-Duct Sound Power Levels

PWL (dB)	Serpentine Inlet	Conventional Inlet	Change
Fan face	174	129	45
AIP	115	97	18
Attenuation	59	32	27

Inlet Distortion Characteristics

The ingestion of the airframe suction surface boundary layer at the cut-back flight free-stream Mach number of 0.1 results in a mass-averaged stagnation pressure deficit of 15% of inlet dynamic pressure. While the pressure recovery is higher at low flight Mach number, the general flow features are in agreement with those obtained by Madani and Hynes for the same inlet at cruise conditions [15]. In particular, the ingested airframe boundary layer and secondary flow effects lead to a pair of streamwise vortices inducing regions of co- and counter-swirl as depicted in Fig. 4 on the right. The asymmetry in the axial Mach number visible on the left side of Fig. 4 is due to the upstream influence of the rotor. It will be shown that the streamwise circulation associated with these vortices strongly affects the rotor blade shock generation and propagation as they alter the rotor inlet relative Mach number distribution.

Inlet Distortion Effect on Shock and MPT Noise Generation

The blade shock strength is governed by the incoming relative Mach number and relative inlet flow angle which can be perturbed by stagger angle changes and more dominantly inlet flow distortion. An unwrapped view of the instantaneous relative Mach number field at 92% span is depicted in Fig. 5 for both the conventional and the serpentine inlet computations, extending from the fan leading edge to the aerodynamic interface plane (AIP).

In the bottom plot small variations in shock strength and angle can be observed due to the blade-to-blade variations in stagger angle. This is the source of MPT noise in undistorted inlet flow. The maximum variation in peak relative Mach number due to the stagger angle variations is 0.04. With inlet distortion present in the top plot, regions with co- and counter-swirl result in relative Mach number variations of as much as 0.32, approximately 8 times larger than the variation due to stagger angle alone. Furthermore, the region of co-swirl leads to subsonic relative Mach numbers (dark blue region) whereas counter-swirl increases the supersonic relative Mach number (yellow region) yielding stronger shocks. This is also manifested in the angle changes of the wave fronts or the corresponding perpendicular wave number vectors: wave fronts inclined further away from the axial direction correspond to increased wave propagation rates while those angled closer to axial propagate at reduced rates, becoming evanescent in the limit of a purely tangential wavenumber vector.

In summary, the non-uniform in-flow condition has a more pronounced effect on shock strength and variation than the stagger angle variations, increasing the amplitude of shaft-order components of the pressure field.

The consequence is an increase in fan sound power level of 45 dB for the serpentine inlet compared to the conventional inlet case. The underlying mechanisms and wave propagation behavior are investigated further in the Analysis Section below.

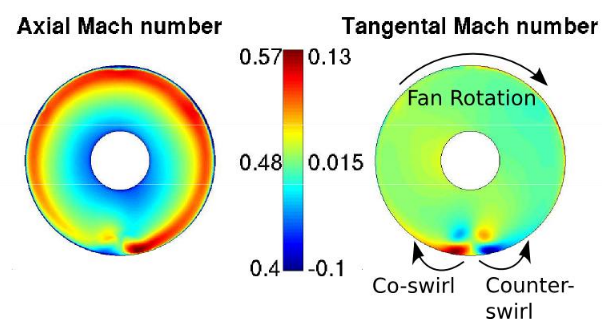

Fig. 4: Axial and tangential Mach number distributions at rotor leading edge for serpentine inlet.

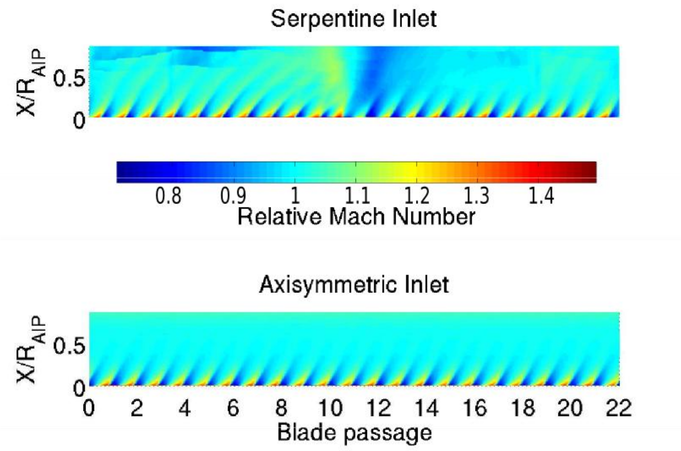

Fig. 5: Relative Mach number at 92% span from fan ($x/R_{AIP} = 0$) to AIP/throat ($x/R_{AIP} = 0.84$)

In-Duct Noise Propagation

To investigate the changes in the acoustic field between the fan face and the AIP, contours of instantaneous unsteady pressure fluctuations are shown in Figs. 6 and 7 for the rotor leading edge and AIP respectively.

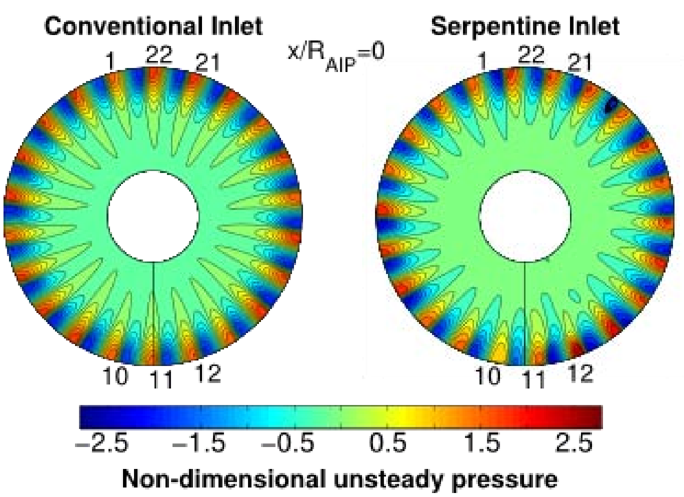

Fig. 6: Unsteady pressure at rotor leading edge over mean dynamic pressure at AIP.

In the conventional inlet case, similar lobed structures, one per blade passage, are visible at both locations near the outer radius. The acoustic modes are comprised of radial and circumferential modes which, on average, are attenuated in amplitude by 27 dB from the fan face to the AIP. A detailed discussion of the modal content can be found in [9]. For the non-uniform inflow case, in addition to the increased sound pressure level, a qualitative change in the unsteady pressure field occurs during upstream propagation. Some of the acoustic modes have decayed at the AIP. This is conjectured to be due to the presence of the subsonic relative flow region induced by the co-swirling streamwise vorticity since the subsonic relative flow should result in locally evanescent wave behavior. Furthermore, the blade-passing circumferential modes are cut-off while a mode with circumferential extent of roughly two blade pitches is dominant and significantly enhanced in sound pressure relative to the rotor leading edge. It should be pointed out that the streamwise vorticity due to boundary layer ingestion is concentrated over about 2 blade pitches, or 1/11th of the circumference. This suggests coupling between the inlet distortion and the duct dynamics, where acoustic modes with spatial frequency equivalent to that of the distortion pattern are excited and scattered.

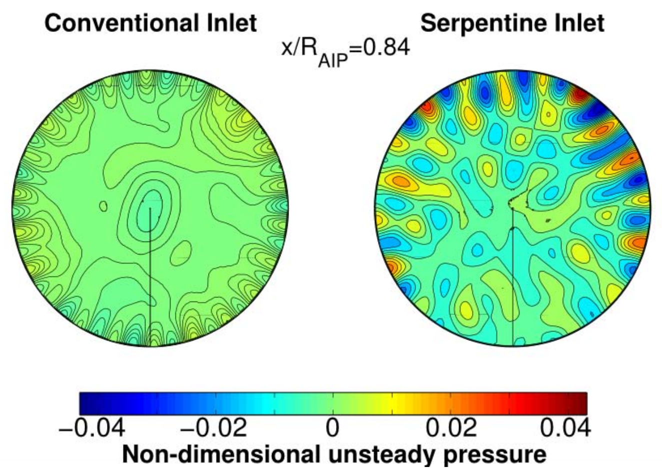

Fig. 7: Unsteady pressure at AIP over mean dynamic pressure at AIP.

For the serpentine inlet, the duct extends further upstream from the AIP and Fig. 8 depicts the unsteady pressure field at the throat near the inlet plane of the serpentine duct. High spatial harmonic modes have vanished and the unsteady pressure field is dominated by long-wavelength, low-frequency waves which remain cut-on. The decay from the AIP to the inlet plane is approximately 15 times less than that from the fan face to the AIP, although the streamwise distance is approximately 4 times longer. The decreased decay rate upstream may be linked to the increasing streamwise vorticity due to vortex stretching as the flow approaches the fan. The small areas of concentrated pressure visible on the lower surface in the figure are numerical effects due to imperfect geometry discretization.

Far-Field Spectra and Overall Noise Levels

The computed and measured spectra at the far-field receiver locations for the conventional inlet case are shown in Fig. 9. All spectra are plotted on a common datum. The computed results have been corrected only for the inherent numerical dissipation of the solver.

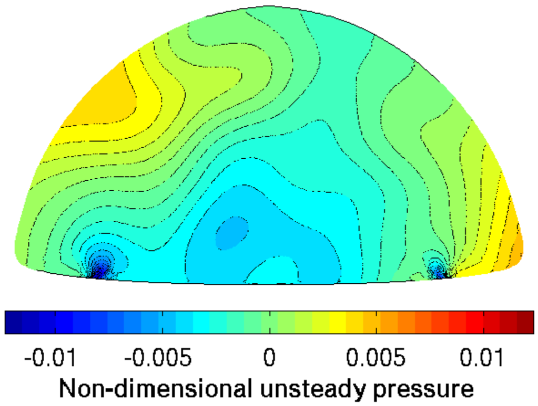

Fig. 8: Unsteady pressure at serpentine inlet throat over mean dynamic pressure at AIP.

The spectra are comprised of multiple-pure tones and the blade passing tone. The levels of the MPTs and in particular the levels relative to the blade-passing tone are generally in agreement. The exact frequencies and amplitude of the MPTs as measured in the experiments are not expected to be reproduced by the computation as the blade stagger angle distribution was not known for the experiments and a random variation was instead assumed. Note that the sound pressure level of the MPTs and the BPF tone decrease for emission angles in excess of 70 degrees. This is conjectured to be due to the proximity of the FW-H surface relative to the nacelle inlet lip. In addition, creeping rays might not be accurately captured, reducing noise levels for observers on the aft arc. The comparison between the conventional and the serpentine inlet are thus conducted on a relative basis.

Fig. 10 depicts the full-scale spectra for the conventional inlet (dashed lines) and serpentine inlet (solid lines) which reveals two striking results for the serpentine inlet case. Firstly, frequencies greater than 11 times the shaft frequency, including the BPF, are absent, suggesting that they are cut-off in the inlet, and the tones are attenuated below the calculation's background noise floor[2]. This is consistent with the sound pressure field observed at the inlet plane shown in Fig. 8. Secondly, the sound pressure level for frequencies less than 11 times shaft frequency are elevated due to the interaction of the inlet flow distortion with the fan rotor and the propagation of acoustic waves through non-uniform background flow. The nature of the mechanism leading to the amplification of the low-frequency tones is investigated in the next Section. While the average linear OASPL is 7dB higher for the serpentine inlet, due to the concentration of acoustic energy at low frequencies, A-weighting the spectra results, on average, in only 3dBA higher OASPL for the serpentine inlet case. It is important to note though that the presence of the airframe acts as a reflecting surface and therefore the A-weighted sound power essentially remains the same for the two cases. The results suggest that, to reduce far-field noise, it may be possible to take advantage of the underlying mechanisms to redistribute the acoustic energy to low frequencies at which the human ear has reduced sensitivity. The results also illustrate that airframe shielding is critical for embedded propulsion system configurations, especially if the source noise is dramatically increased. Lastly, returning to Fig. 5 and the observation made earlier that the inlet distortion is primarily confined to two blade pitches, or 1/11th of the circumference, it is interesting to note that the tones in the far-field are absent at approximately 11 times shaft frequency and above. The next Section explores how much of this effect is due to source noise changes from inlet distortion versus the sound propagation through non-uniform flow.

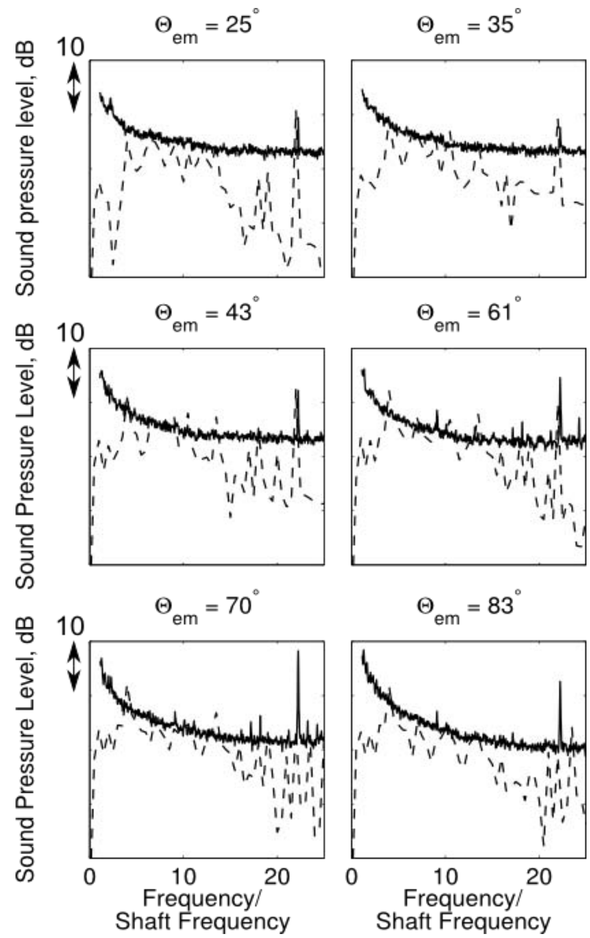

Fig. 9: Linear far-field spectra (dashed lines: computation; solid lines: experimental data).

[2] Fan broadband noise is not modeled in the simulations and the background noise floor is therefore set by numerical noise.

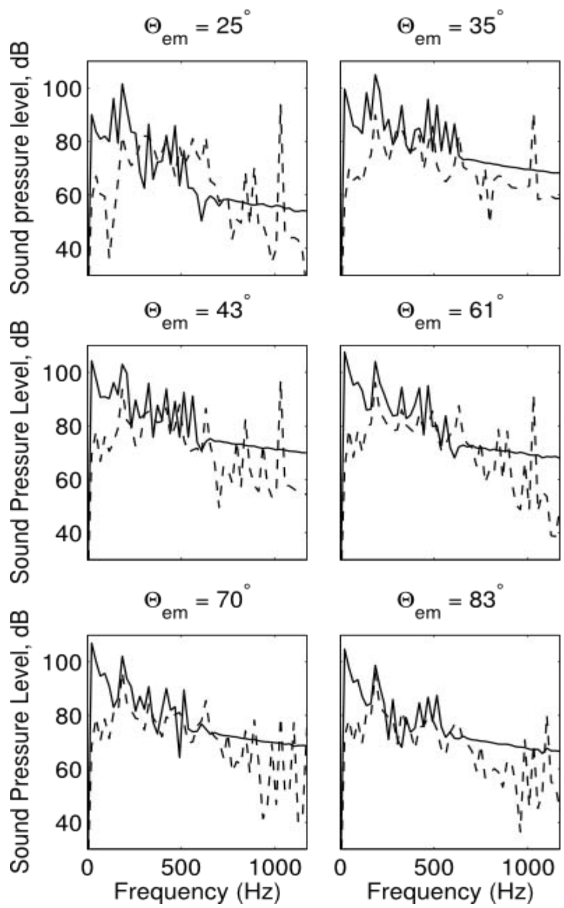

Fig. 10: Full-scale linear far-field spectra (dashed lines: conventional inlet; solid lines: serpentine inlet).

ANALYSIS OF INLET DISTORTION EFFECTS ON SHOCK STRENGTH AND LINEAR WAVE PROPAGATION

In light of the results discussed above, a simplified model is used to illustrate the underlying mechanisms and links between inlet swirl distortion, increased shock strength and related MPT noise, and cut-off wave behavior. As discussed earlier, at the cut-back fan operating condition considered here, the rotor blade tips experience supersonic inflow conditions with detached shocks where the unchoked blade passage mass flow is governed by the rotor inlet relative Mach number M_1 and the relative inlet flow angle β_1. This is shown in Fig. 11.

With inlet flow distortion present, the inlet relative Mach number and flow angle into the blade passages that pass through the stationary region of inlet swirl are perturbed, leading to variations in passage inflow conditions and thus shock strength and location. Even for perfectly identical blades, the resulting spillage from one blade passage to another yields a non-axisymmetric shock distribution leading to multiple-pure tone noise. While this complicated flow field and passage-to-passage interaction can only be captured in a numerical simulation such as was done above, the simplified model described below is useful to guide the interrogation of the resulting shock strength variation. Assuming small perturbations, the evanescent and propagating wave behavior due to a non-axisymmetric modulation in shock strength can also be investigated. The model is based on the control volume formulation by Freeman and Cumpsty [20] marked by the dashed line in Fig. 11.

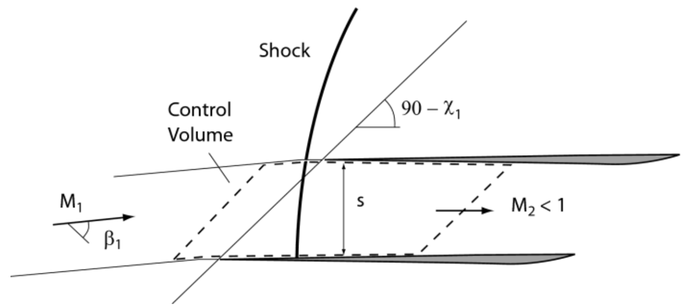

Fig. 11: Control volume analysis for detached shock strength (adapted from [20]).

The underlying idea is that in the limit of an infinitesimally small blade pitch (neglecting blade thickness and $s \rightarrow 0$) the unchoked flow field in the blade tip region becomes axisymmetric with a circumferentially uniform shock surface[3] as sketched in the middle part of Fig. 12. Conservation of mass, rothalpy, and momentum along the blade passage yield

$$\begin{aligned} \rho_1 V_1 \cos\beta_1 &= \rho_2 V_2 \cos\chi_1 \\ T_1\left(1+\frac{\gamma-1}{2}M_1^2\right) &= T_2\left(1+\frac{\gamma-1}{2}M_2^2\right) \\ p_1\cos\chi_1 + p_1\gamma M_1^2\cos\beta_1\cos(\chi_1-\beta_1) &= p_2\cos\chi_1 + p_2\gamma M_2^2\cos\chi_1 \end{aligned} \quad (3)$$

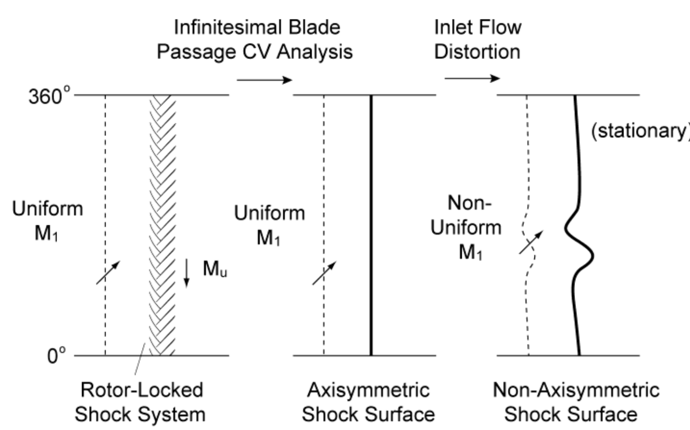

Fig. 12: Modulated shock surface model.

[3] This is consistent with the assumptions used in the body force representation of axisymmetric through-flow for identical blade passages.

For given inflow conditions M_1 and β_1 and blade leading edge camber angle χ_1, the above set of equations can be solved for the downstream conditions and thus the shock surface static pressure ratio p_2 / p_1 can be determined. For a fixed geometry, there are inflow conditions for which the above equations do not have a solution, indicating that the flow is choked.

Returning to the problem at hand, the inlet flow distortion yields streamwise vortices which lead to co- and counter-swirl manifested in regions of subsonic and supersonic relative blade inlet Mach numbers (see Fig. 13).

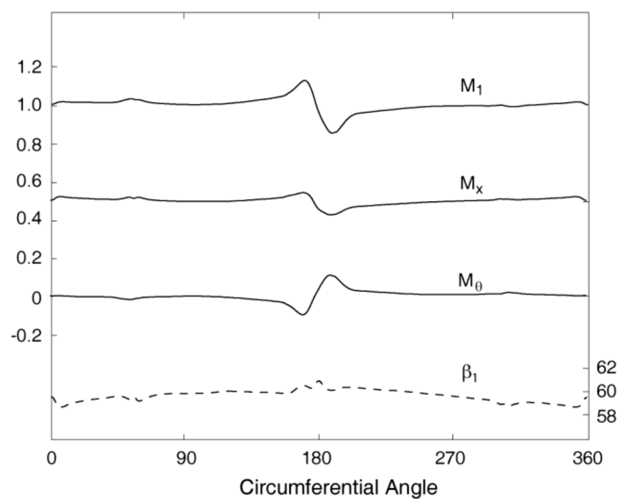

Fig. 13: Computed Mach numbers and relative flow angle at 92% span at rotor leading edge for serpentine inlet case.

For the flow conditions investigated here, the circumferential variation in relative inlet Mach number is dominant compared to the corresponding relative flow angle changes such that, using the above model, the shock surface strength depends predominantly on M_1 and $p_2 / p_1(M_1, \beta_1) \approx \pi_{12}(M_1)$ as shown Fig. 14. Though the incoming relative flow is subsonic at the low end of the curve depicted in the figure, there is still a static pressure rise since the relative flow Mach number decreases as the flow enters the blade passage. The variation in relative Mach number around the circumference is schematically depicted in the inset leading to a peak-to-peak modulation in shock surface strength of $\Delta\pi_{12} = 0.3$.

Assuming now that the blade-to-blade pressure variation is a rotor-locked sawtooth distribution $N(\theta + \Omega t)$ of unit strength, the modulated rotor-locked static pressure ratio distribution becomes

$$\pi_{12}(\theta,t) = \pi_{12}(\theta)N(\theta + \Omega t) \tag{4}$$

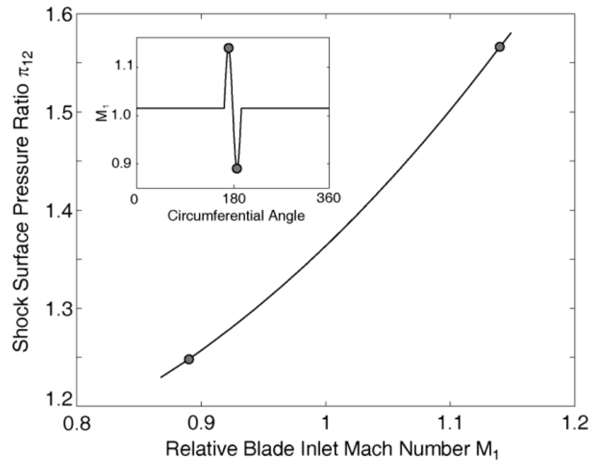

Fig. 14: Shock strength dependence on relative Mach number; inset: inlet distortion as idealized relative Mach number distribution.

For simplicity, it is assumed that the stagnation pressure upstream is uniform[4]. The peak-to-peak rotor-locked pressure variation $\Delta p_{21} = p_2 - p_1$ is then readily determined and can be written in terms of a modulated spatial Fourier series

$$\Delta p_{21}(\theta,t) = \sum_{m=0}^{\infty} P_m e^{jm\theta} \sum_{n=1}^{\infty} C_n e^{jnB(\theta+\Omega t)} \tag{5}$$

where B is the rotor blade count. The first Fourier series represents the modulation of the stationary shock surface while the second series is the decomposition of the rotor-locked sawtooth pressure pattern. This is illustrated schematically in Fig. 15. The modulated shock strength induces non-zero modal amplitudes in shaft-order (and harmonics) spatial modes which are not present in the uniform inflow case.

Returning to the observation that with inlet distortion frequencies higher than 11 times the shaft frequency appear to be cut-off in the far-field spectra, the question arises as to how the wave propagation behavior upstream of the rotor is altered due to the modulated shock surface strength. While the propagation of acoustic waves through the non-uniform mean flow in the serpentine duct is complicated, the analysis can be used to investigate the linear wave behavior in the near field of the rotor where the duct outer radius is approximately constant. Assuming small perturbations, uniform background flow in the axial direction, and neglecting radial variations, the two-dimensional convective wave equation can be written for a periodic domain as

$$\frac{1}{c^2}\left(\frac{\partial}{\partial t} + \bar{u}_x \frac{\partial}{\partial x}\right)^2 \delta p - \frac{\partial^2 \delta p}{\partial x^2} - \frac{1}{R^2}\frac{\partial^2 \delta p}{\partial \theta^2} = 0 \tag{6}$$

[4] This is deemed appropriate as the inlet pressure recovery is 99% at the low cut-back flight Mach number of 0.1.

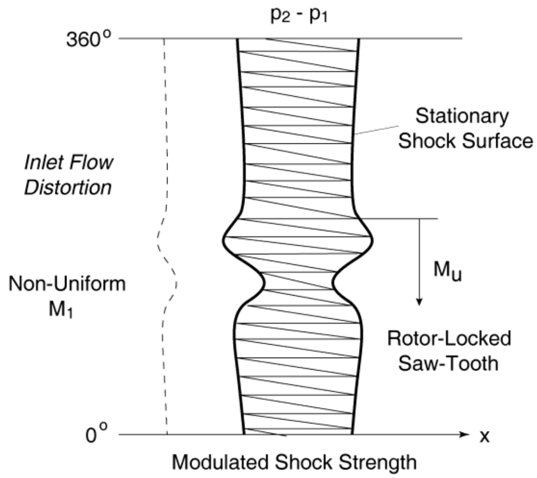

Fig. 15: Rotor-locked sawtooth wave modulated by stationary shock surface in non-uniform flow.

The solution to the above equation will be of the form

$$\delta p(x,\theta,t) = \sum_{m=0}^{\infty}\sum_{n=1}^{\infty} g_{mn}(x) e^{j[m\theta + nB(\theta+\Omega t)]} \tag{7}$$

Note the presence of the $e^{jm\theta}$ term, which appears as a result of the distorted inflow and is not time-dependent. Substituting this into Eq. 6 yields a second order differential equation for g_{mn}:

$$\begin{aligned}&\left(1-M_x^2\right)\frac{d^2 g_{mn}(x)}{dx^2} - 2j\frac{nB}{R}M_x M_u \frac{dg_{mn}(x)}{dx} + \\ &\left[\left(\frac{nB}{R}\right)^2\left(M_u^2-1\right) - \left(\left(\frac{m}{R}\right)^2 + \frac{2mnB}{R^2}\right)\right] g_{mn}(x) = 0\end{aligned} \tag{8}$$

where $M_1 = \sqrt{M_x^2 + M_u^2}$. With the known rotor pressure field at $x = 0$ and invoking Sommerfeld's irradiation condition far upstream, the solution for $x < 0$ becomes

$$g_{mn}(x) = \Lambda_{mn} e^{jk_x x} \tag{9}$$

where $\Lambda_{mn} = P_m C_n$ and the axial wavenumber yields

$$k_x = \frac{nB}{R}\left(\frac{M_x M_u - j\sqrt{\left(\frac{m}{nB}+1\right)^2\left(1-M_x^2\right) - M_u^2}}{1-M_x^2}\right) \tag{10}$$

Evanescent wave behavior is obtained when the square root remains real and therefore wave propagation is cut-off for

$$\frac{m}{nB} + 1 > \frac{M_u}{\sqrt{1-M_x^2}} \tag{11}$$

For a uniform shock surface strength (no distortion, $m = 0$ only), the familiar wave propagation condition $M_1 > 1$ is recovered and modes are cut-on for supersonic relative blade inlet Mach numbers. With inlet flow distortion the shock surface strength is non-uniform ($m \geq 0$) and the cut-on behavior depends on the reduced spatial frequency, m/nB. For values much less than one, the behavior approaches the uniform inflow case whereas for values close to one, where the length scale of the shock strength variation is of order blade pitch, modes can be cut-off even if the relative inlet Mach number is supersonic. For the serpentine inlet flow conditions in the computations discussed above, the maximum inlet relative Mach number near the blade tips is 1.1 and the axial Mach number is approximately 0.5. Therefore in order for a mode to be cut-off, the reduced spatial frequency must satisfy

$$\frac{m}{nB} > 0.13 \tag{12}$$

Since $B = 22$ for the NASA/GE R4 rotor investigated here, the cut-off condition becomes $m > 2n$. Considering the lowest harmonic $n = 1$, the analysis suggests that any shock surface modulation of spatial harmonic extent greater than $m = 2$ can lead to cut-off behavior. For the type of inlet distortion observed in the simulation, the fundamental component of the distortion $P_{m=0}$ is typically larger than $P_{m>0}$ by at least an order of magnitude. With this, the simplified model suggests that, since $I_{mn} \propto \Lambda_{mn}^2$, the net increase in sound intensity relative to uniform inflow is negligible. It must therefore be concluded that, for small perturbations, a linearized shock surface modulation in a uniform background flow does not by itself yield the observed 45 dB increase in fan rotor sound power level. It is therefore conjectured that the combination of non-uniform shock surface strength and the propagation of sound through non-uniform inflow results in the computed increase in sound power.

Furthermore, the simplified model was restricted to blade passing frequencies and since their acoustic energy at BPF is essentially unchanged in the presence of inlet distortion, the attenuation of the BPF tone in the full simulation (and likely the MPTs above 11 times shaft frequency as well) is suggested to be due to the propagation through the non-uniform flow in the serpentine inlet. This mechanism is also deemed to be responsible for the elevated amplitudes of the tones below 11 times shaft frequency as acoustic energy can be redistributed in non-uniform flow.

The take-away message from this analysis is that non-uniform flow affects the acoustic propagation more dominantly than the source noise generation. In order to accurately capture this effect, simulations such as those employed above are required. Work is currently underway using full domain non-linear simulations to further investigate the influence of the non-uniform background flow on source noise generation and wave propagation.

CONCLUSIONS & OUTLOOK

The generation and propagation of rotor-alone tones in both conventional and serpentine inlet ducts have been investigated. A new methodology for the coupled aeroacoustic assessment of MPT noise using an innovative implementation of a body-force-based rotor model was employed. The non-uniform flow in the serpentine inlet results in a 45dB increase in sound power at the fan face relative to the uniform flow condition. In the far-field, however, the average increase in OASPLs at the receiver locations is only 7dB or 3dBA. The far-field spectra differ significantly for the two cases. Compared to the conventional inlet, the serpentine inlet results have higher SPLs at frequencies less than one-half BPF, while tones above this frequency appear to be cut-off. Examination of the inlet distortion pattern in the vicinity of the fan leading edge revealed that the frequency above which tones are absent in the far-field appears to be related to the circumferential extent of the distortion. A simplified model of the rotor noise source generation in non-uniform flow was presented which corroborates the circumferential variation in shock strength due to inlet distortion. The presence of inlet distortion energizes higher-order circumferential modes at the BPF in the model. A linearized wave propagation analysis based on this model provides criteria for propagating modes and indicates that the increase in source sound power, the amplification of tones below one-half BPF and the apparent cut-off of tones above this frequency are predominantly governed by acoustic propagation effects through the non-uniform flow rather than by inlet distortion effects on source noise. This motivates a parametric study of duct geometries in order to determine the dependence of the far-field spectra on inlet distortion characteristics.

The parametric study, involving circular cross-section serpentine inlets, is currently underway in order to quantitatively relate in-duct flow features, such as the streamwise and circumferential pressure gradients, to source noise generation and propagation for rotor-alone tone noise. The parameter space explored covers duct offsets of 0.25 to 0.75 fan diameters and duct area ratios of 1.01 to 1.05, ensuring sufficient changes in the duct flow field to significantly affect sound propagation through the non-uniform flow. A key outcome of this study will be a response surface model for the acoustic behavior as a function of the time-mean flow features in the inlet duct, enabling the estimation of rotor-alone noise in advanced aircraft configurations with BLI.

ACKNOWLEDGMENTS

The authors would like to thank Professor Nick Cumpsty and Dr. John Adamczyk for their helpful comments and discussions. Special thanks go to Dr. Ed Envia of NASA Glenn for his assistance in obtaining the R4 rotor geometry and acoustic measurement data. This research was funded by the NASA Langley Research Center, Dr. Russell Thomas contract monitor.

REFERENCES

[1] Sargeant, M., 2007, "Boundary Layer Ingestion for Advanced Airframes," Ph.D. Thesis, University of Cambridge.
[2] Berrier, B., and Allan, B., 2004, "Experimental and Computational Evaluation of Flush-Mounted, S-Duct Inlets," AIAA 2004-0764.
[3] Gliebe, P., Mani, R., Shin, H., Mitchell, B., Ashford, G., Salamah, S., and Connel, S., 2000, "Aeroacoustic Prediction Codes," NASA CR-2000-210244.
[4] Mathews, D., and Nagel, R., 1973, "Inlet Geometry and Axial Mach Number Effects on Fan Noise Propagation," AIAA 1973-1022.
[5] Prasad, D., and Feng, J., 2005, "Propagation and Decay of Shock Waves in Turbofan Engine Inlets," J. Turbomachinery, **127**(1), pp. 118-127.
[6] Coupland, J., Wilson, A., Pollard, N., Uellenberg, S., Breard, C., and Diamond, J., 2007, "Demonstration of a CFD-CAA Methodology to Predict Buzz-Saw Noise Propagation to the Aircraft," AIAA 2007-3517.
[7] Brambley, E., and Peake, N., 2007, "Sound in Curved Intakes," AIAA 2007-3552.
[8] Brambley, E., and Peake, N., 2008, "Sound Transmission in Strongly Curved Slowly Varying Cylindrical Ducts with Flow," J. Fluid. Mech. **596**, pp. 287-412.
[9] Defoe, J., Narkaj, A., and Spakovszky, Z., 2010, "A Body-force-based Method for Prediction of Multiple-Pure-Tone Noise: Validation," AIAA 2010-3747.
[10] Defoe, J., Narkaj, A., and Spakovszky, Z., 2009, "A Novel MPT Noise Methodology for Highly-Integrated Propulsion Systems with Inlet Flow Distortion," AIAA 2009-3366.
[11] Podboy, G., Krupar, M., Helland, S., and Hughes, C., 2002, "Steady and Unsteady Flow Field Measurements Within a NASA 22 Inch Fan Model," AIAA 2002-1033.
[12] Hughes, C., Jeracki, R., Woodward, R., and Miller, C., 2002, "Fan Noise Source Diagnostic Test – Rotor Alone Aerodynamic Performance Results," AIAA 2002-2426.
[13] Woodward, R., Hughes, C., Jeracki, R., and Miller, C., 2002, "Fan Noise Source Diagnostic Test – Far-field Acoustic Results," AIAA 2002-2427.
[14] Heidelberg, L, 2002, "Fan Noise Source Diagnostic Test – Tone Modal Structure Results," AIAA 2002-2428.
[15] Madani, V., and Hynes, T., 2009, "Boundary Layer Ingesting Intakes: Design and Optimization," ISABE 2009-1346.
[16] Hileman, J., and Spakovszky, Z., and Drela, M., 2010, "Airframe Design for Silent Fuel-Efficient Aircraft," J. Aircraft, **47**(3), pp. 956-969.

[17] Huttl, T., Kahl, G., Kennepohl, F., and Heinig, K., 2001, "Resolution Requirements for the Numerical Computation of Tonal Noise in Compressors and Turbines of Aeroengines," RTO AVT Symp. Ageing Mech. And Control.
[18] Freund, J., 1997, "Proposed Inflow/Outflow Boundary Condition for Direct Computation of Aerodynamic Sound," AIAAJ, **35**(4), pp. 740-742.
[19] Sutliff, D., 2005, "Rotating rake turbofan duct mode measurement system," NASA/TM-2005213828.
[20] Freeman, C., and Cumpsty, N., 1992, "A Method for the Prediction of Supersonic Compressor Blade Performance," J. Propulsion and Power, **8**(1), pp. 199-208.

